



Thermodynamic mixing properties of disordered alkali feldspar solid-solution from Na–K partitioning and low-temperature calorimetry

D. Heuser¹ · E. Petrishcheva¹ · F. Ingegneri¹ · C. L. Lengauer² · E. Dachs⁴ · C. Hauzenberger³ · R. Abart¹

Received: 3 November 2023 / Accepted: 10 January 2024 / Published online: 26 February 2024
© The Author(s) 2024

Abstract

The equilibrium partitioning of Na and K between alkali feldspar and NaCl–KCl salt melt was determined at 800 °C, 850 °C, 900 °C, 950 °C and 1000 °C and close to ambient pressure. Four different natural gem-quality alkali feldspars with low degree of Al–Si ordering covering the range from orthoclase to high sanidine and with slightly different minor element concentrations were used as starting materials. The partitioning curves obtained for the four feldspars are indistinguishable indicating that Na–K partitioning independent of the differences of Al–Si ordering state and minor element concentrations existing amongst these feldspars. A sub-regular two parameter Margules type solution model was fitted to the partitioning data, and the excess Gibbs energy describing the thermodynamic non-ideality of the alkali feldspar solid-solution and the respective Margules parameters W_{gK} and W_{gNa} including their temperature dependence expressed as $W_g = W_h - TW_s$ were determined:

$$W_{gK} = 19754 \pm 3140J \cdot \text{mol}^{-1} - T \cdot 2.33 \pm 2.67J \cdot \text{mol}^{-1} \cdot K^{-1}$$
$$W_{gNa} = 14916 \pm 4272J \cdot \text{mol}^{-1} - T \cdot 3.55 \pm 3.64J \cdot \text{mol}^{-1} \cdot K^{-1}$$

The corresponding solvus has a critical temperature slightly above 650 °C and is well comparable with earlier direct experimental determinations of the low-sanidine-albite solvus curve. Comparison of the vibrational excess entropy determined from low-temperature heat capacity measurements with the total excess entropy derived from the temperature dependence of the excess Gibbs energy yields a negative configurational contribution to the excess entropy pointing towards short-range Na–K ordering on the alkali site.

Keywords Alkali feldspar solid-solution · Thermodynamic mixing properties · Na–K partitioning experiments · Low-temperature calorimetry · Excess Gibbs energy

Introduction

Feldspar is the most abundant mineral in Earth's crust. The composition of feldspar with respect to its major components may be described in the ternary system $\text{CaAl}_2\text{Si}_2\text{O}_8$ – $\text{NaAlSi}_3\text{O}_8$ – KAlSi_3O_8 . The latter two components define the composition space of alkali feldspar, which is a solid-solution between the albite ($\text{NaAlSi}_3\text{O}_8$) and K-feldspar (KAlSi_3O_8) end-members. In the crystal structure of alkali feldspar, Al and Si are tetrahedrally coordinated by four oxygen ions forming a framework of corner sharing AlO_4 and SiO_4 tetrahedra. The alkali cations occupy large, irregularly coordinated cavities in the tetrahedral framework. Four non-equivalent tetrahedral sites are discerned: T_1m , T_{10} , T_{2m} and T_{2o} . In disordered alkali feldspar Al^{3+} and

✉ D. Heuser
david.heuser@univie.ac.at

¹ Department of Lithospheric Research, University of Vienna, Vienna, Austria

² Department of Mineralogy and Crystallography, University of Vienna, Vienna, Austria

³ Department of Earth Sciences, University of Graz, Graz, Austria

⁴ Department of Chemistry and Physics of Materials, University of Salzburg, Salzburg, Austria

Si^{4+} are randomly distributed over all four tetrahedral sites. Preferential partitioning of Al^{3+} on to the T_1 sites relative to the T_2 sites, where $T_1 = T_{1m} + T_{1o}$ and $T_2 = T_{2m} + T_{2o}$, and finally, preferential partitioning of Al^{3+} on T_{1o} over T_{1m} leads to successively more ordered configurations. We adopt the scheme of Ribbe (1983) for the classification of alkali feldspars with different states of Al–Si ordering. For details please refer to the Supplementary Information.

At high temperatures - above about 650 °C for Al–Si-disordered and above about 900 °C for ordered alkali feldspar - a continuous solid-solution exists between the Na and K end-members. Towards lower temperatures a miscibility gap opens due to the thermodynamic non-ideality of the alkali feldspar solid-solution. The thermodynamics of the alkali feldspar solid-solution has been addressed by several authors. Direct determinations of the alkali feldspar solvus have been provided by Bachinski and Müller (1971) for ordered alkali feldspars corresponding to the low-albite - microcline series and by Luth and Tuttle (1966), Smith and Parsons (1974), Lagache and Weisbrod (1977) and Parsons (1978) for disordered, topochemically monoclinic alkali feldspars. High pressure solvus experiments in the range of 9 to 15 kbar were provided by Goldsmith and Newton (1974). Ion exchange experiments between alkali feldspar and aqueous solutions were performed at 200 MPa by Orville (1963). The Na–K partitioning between alkali feldspar and (K, Na) Br or (K, Na) Cl salt melt were determined for the low-albite - microcline series by Delbove (1975) and for the analbite - sanidine series, high sanidine after Ribbe (1983), and the adularia (orthoclase) based series by Hovis et al. (1991) and by Neusser et al. (2012).

The enthalpies of the alkali feldspar solid-solution series prepared by cation exchange from alkali feldspar starting materials with different Al–Si ordering states were determined by solution calorimetry (Hovis 1988, 2017), and the vibrational entropies of alkali feldspar solid-solutions were determined from low-temperature calorimetric heat capacity measurements for disordered alkali feldspars of the analbite-sanidine series by Haselton et al. (1983) and for the low-albite - microcline series by Benisek et al. (2015). The compositional dependence of molar volumes of the alkali feldspar solid-solution was determined from powder and single crystal X-ray diffraction data (Orville 1967; Waldbaum and Thompson 1968; Kroll et al. 1986; Hovis 2017).

The current status of knowledge on the thermodynamic mixing properties of the alkali feldspar solid-solution can be summarised as (Hovis 2017): (i) The alkali feldspar solvus is asymmetric with the critical composition between $X_K = 0.3$ and 0.4 , where X_K is the site fraction of K on the alkali site. (ii) The critical temperature of the alkali feldspar solvus increases with increasing Al–Si ordering. (iii) Accordingly, the excess Gibbs energy, g^{ex} , is asymmetric with the

maximum at X_K between 0.38 and 0.44 and maximum values of g^{ex} in the range of 3.0 – 3.5 kJ/mol. (iv) The vibrational excess entropy of mixing $s^{\text{ex,vib}}$ obtained from calorimetric data is higher than the total excess entropy s^{ex} of mixing obtained from phase equilibrium data implying the presence of negative excess configurational entropy $s^{\text{ex,con}}$, which may arise from short range ordering or clustering of Na^+ and K^+ on the alkali sites.

This understanding was derived from combining information from different types of phase equilibrium experiments as well as solution and low-temperature calorimetry measurements. The basic data have been obtained from different feldspars with different Al–Si ordering and trace element contents, both characteristics are partially unknown for the different experiments. Moreover, solvus curves were determined at different pressures, using different starting materials and different experimental techniques and may not be fully comparable.

Thus, despite numerous studies, knowledge of the thermodynamics of the alkali feldspar solid-solution is still limited, and considerable uncertainty with regard to the thermodynamic mixing properties has remained. In this study, we determined the Na–K equilibrium partitioning between natural gem-quality alkali feldspar and NaCl–KCl salt melt under close to ambient pressure and at five different temperatures. We used four different alkali feldspars with slightly different minor and trace element compositions and Al–Si ordering as starting materials applying the exact same experimental procedure for each sample. This ensures direct comparability of the results from the different feldspars and identification of the impact of the degree of Al–Si order and of minor element contents on the excess Gibbs energy. Moreover, it allows for determining s^{ex} from the temperature dependence of g^{ex} and to obtain $s^{\text{ex,con}}$ from the difference between s^{ex} and $s^{\text{ex,vib}}$, which was determined for two of the investigated feldspars by low-temperature heat capacity measurements.

Methods

Starting material

Four different K-rich alkali feldspars were used as starting materials: Madagascar Orthoclase (M) (actually low sanidine) from Itrongay, Madagascar, Volkesfeld Sanidine (V) from the Eifel, Germany, Zillertal Adularia (Z) from Zillertal, Austria, and Zinggenstock Adularia (Zg) from Guttannen, Switzerland. All four feldspars are homogeneous and featureless under the light and scanning electron microscope. Madagascar Orthoclase is yellow and Volkesfeld Sanidine greyish-brown, both are transparent. Zillertal Adularia and Zinggenstock Adularia are milky white, 1 mm thick pieces are translucent and colourless (see Fig. S1). For all four

feldspars major and trace element concentrations, lattice parameters and the state of Al–Si ordering were determined. For details see the (Fig. S3 and Table S2).

Experimental procedure

Each feldspar was crushed to a powder and sieved. The 63–100 μm fraction was used for the partitioning experiments. About 15 mgs of feldspar powder was mixed with NaCl and KCl salt, where the amount of salt was chosen so that a 40:1 molar proportion of the alkali cations in the salt relative to the feldspar and a certain KCl mole fraction X_{KCl} in the salt was obtained. For details please refer to the Supplementary Information.

For each feldspar and each temperature 12–15 different salt compositions were used to constrain the partitioning over the entire compositional range of alkali feldspar. The salt-feldspar mixtures were then sealed in evacuated quartz glass tubes, shaken for a better mixing of feldspar and salt and kept at 800 °C, 850 °C, 900 °C or 950 °C for 35 days or at 1000 °C for 28 days in box furnaces at close to atmospheric pressure. Different run durations had been tested beforehand to determine the time needed for complete compositional homogenization throughout the feldspar grains. In addition, experiments were run for each feldspar at 1000 °C for 28 days and at 900 °C for 35 days to check via pXRD analyses, to what extent the state of Al–Si ordering changes during annealing.

After the exchange experiments, the samples were quenched in cold water, and the glass tubes were checked for tightness. Those which had remained tight after quenching were opened and rinsed with purified water to separate the feldspar powder from the salt. The feldspar powder was then mounted in phenolic resin with graphite filler, polished and carbon coated for electron probe micro analysis (EPMA). All experimental runs are listed in Table 2.

EPMA and ICP-MS analysis

All samples were analysed with a Cameca SX Five electron probe micro analyser (EPMA) at the Department of Lithospheric Research, University of Vienna. 15 kV acceleration voltage and 20 nA beam current were applied, and each element was calibrated on natural mineral standards. The beam was defocused to 6 μm diameter to minimise sample damage and loss of sodium through evaporation. Trace element concentrations were analysed using inductively coupled plasma mass spectrometry (ICP-MS, Agilent 7500) at the Institute of Earth Sciences, University of Graz (Austria). For details please refer to the Supplementary Information.

pXRD

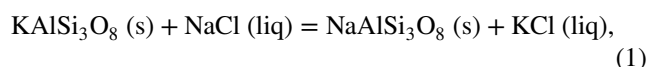
Powder X-ray diffraction (pXRD) was performed on the starting material and on feldspar that was annealed at 900 °C for 35 days and shifted to different compositions to analyse changes in Al–Si order with thermal annealing and with cation exchange. For the analyses, the feldspar powder was further ground to smaller grain sizes to reduce texture effects. The pXRD measurements were carried out using CuK α radiation on a Philips PW3020 diffractometer at the Department of Mineralogy and Crystallography, University of Vienna. Rietveld refinement was employed for extracting lattice parameters using the TOPAS-6 software.

Relaxation calorimetry

The heat capacities of 14 samples along the sanidine - high-albite solid solution series prepared from V and of five samples prepared from M were measured in the temperature range of 2–300 K by relaxation calorimetry using a Physical Property Measurement System (PPMS) by Quantum Design at Salzburg University. To this end, 10–20 mg milligrammes of feldspar powder with grain size 100–200 μm were compacted and wrapped into a thin Al foil, pressed into discs and loaded into the calorimeter. Heat capacities between 2 and 300 K were then measured at 60 logarithmically spaced temperature set points in triplicate. For details on the calorimetric measurements the reader is referred to Dachs and Bertoldi (2005).

Thermodynamic analysis of partitioning data

For the exchange of Na and K between alkali feldspar and NaCl–KCl salt melt, the exchange reaction



may be written, where (s) and (liq) indicate solid and liquid phases, respectively. Equilibrium partitioning of Na and K between feldspar and salt melt requires (Thompson and Waldbaum 1968)

$$\Delta_r g = 0 = \Delta_r g^0 + RT \ln \left(\frac{X_{\text{Na}} \gamma_{\text{Na}} X_{\text{KCl}} \gamma_{\text{KCl}}}{X_{\text{K}} \gamma_{\text{K}} X_{\text{NaCl}} \gamma_{\text{NaCl}}} \right) \quad (2)$$

where $\Delta_r g^0$ is the Gibbs energy change of the reaction amongst the end members, X_{Na} , X_{K} are the site fractions of Na and K on the alkali site of the feldspar and X_{NaCl} , X_{KCl} are the mole fractions of NaCl and KCl in the salt melt. The γ_i parameters are the respective activity coefficients. Based on an asymmetric Margules model (Margules 1895; Thompson 1967) the latter can be described as

$$RT\ln\gamma_A = X_B^2[W_{gA} + 2(W_{gB} - W_{gA})X_A] \tag{3}$$

$$RT\ln\gamma_B = X_A^2[W_{gB} + 2(W_{gA} - W_{gB})X_B],$$

where A and B refer to K and Na for the alkali feldspar and to KCl and NaCl for the salt melt. For KCl–NaCl salt melt Margules parameters W_{gKCl} and W_{gNaCl} are available from Hersh and Kleppa (1965) and Yin et al. (2020). At the temperatures of interest, the non-ideality of the salt melt is minute, and partitioning curves calculated with ideal mixing in the salt melt yield slightly better fits to the measured feldspar compositions than when non-ideality in the salt melt is considered. Therefore, for extracting Margules parameters for the feldspar mixing model, γ_{KCl} and γ_{NaCl} in Eq. (2) were set to unity. Inserting Eq. (3) into Eq. (2) yields

$$-RT\ln\left(\frac{X_{Na}X_{KCl}}{X_KX_{NaCl}}\right) = W_{gK}(-X_{Na}^2 + 2X_{Na}X_K^2 + 2X_{Na}^2X_K) + W_{gNa}(X_K^2 - 2X_{Na}X_K^2 - 2X_{Na}^2X_K) + \Delta_r g^0 \tag{4}$$

This equation must hold for the Na–K partitioning of every feldspar - salt-melt pair. Each partitioning experiment yields the compositions of salt and feldspar that coexist in equilibrium at a given temperature, and only the two Margules parameters and $\Delta_r g^0$ are the unknowns. We used the equilibrium partitioning data from 40 to 60 feldspar-melt pairs for each temperature and applied the least square method to simultaneously satisfy the respective 40–60 equations Eq. (4) to obtain the best-fit W_{gK} and W_{gNa} parameters and $\Delta_r g^0$ for each temperature.

The corresponding partitioning curves are obtained from rearranging Eq. (4) to

$$X_{KCl} = \left[\frac{X_{Na}}{X_K} \exp\left(\frac{W_{gK}(-X_{Na}^2 + 2X_{Na}X_K^2 + 2X_{Na}^2X_K) + W_{gNa}(X_K^2 - 2X_{Na}X_K^2 - 2X_{Na}^2X_K) + \Delta_r g^0}{RT}\right) + 1 \right]^{-1} \tag{5}$$

and inserting the best-fit Margules parameters and $\Delta_r g^0$ for each temperature. Only the results obtained based on the assumption of ideal mixing in the salt melt are presented and discussed here. For comparison, results obtained from calculations including non-ideal mixing in the salt melt are shown in the Supplementary Information (Fig. S5). In addition, $\Delta_r g^0$ was calculated from thermodynamic data of Holland and Powell (1998), upgrade 5.5 (ds55) using PerpleX (Connolly 2005), which yielded values for $\Delta_r g^0$, which are close to those obtained from the least square fit and, accordingly, almost identical partitioning curves. The $\Delta_r g^0$ values calculated from the dataset of Holland and Powell (2011) (ds633) are, however, not suited for reproducing our partitioning data potentially indicating a disconnection between

silicate and halide data in the latest version of the thermodynamic data set (see Fig. S6 and Table S3).

The W_{gNa} and W_{gK} parameters obtained for the different temperatures show a moderate decrease with increasing temperature (Fig. 1). Making use of the relation (Thompson and Waldbaum 1968; Thompson 1967)

$$W_g = W_h - W_s T \tag{6}$$

the W_{hK} , W_{sK} , W_{hNa} and W_{sNa} parameters were extracted from linear fits of W_{gNa} and W_{gK} versus temperature. The resulting excess molar enthalpy and molar entropy functions were obtained from (Thompson 1967; Thompson and Waldbaum 1968)

$$g^{ex} = X_K X_{Na} (W_{gK} X_{Na} + W_{gNa} X_K)$$

$$h^{ex} = X_K X_{Na} (W_{hK} X_{Na} + W_{hNa} X_K) \tag{7}$$

$$s^{ex} = X_K X_{Na} (W_{sK} X_{Na} + W_{sNa} X_K).$$

The corresponding solvus curve was calculated based on

$$g^{sol} = RT(X_{Na} \ln X_{Na} + X_K \ln X_K) + X_K X_{Na} (W_{gK} X_{Na} + W_{gNa} X_K) \tag{8}$$

using Gibbs energy minimisation. It must be noted, that the run products are likely metastable with respect to their Al–Si ordering state, as attainment of equilibrium Si–Al distribution is not very likely to occur over the time scales of the cation exchange experiments.

Thermodynamic analysis of calorimetric data

Heat capacities from low-temperature calorimetric meas-

urements were used to calculate the vibrational entropy s^{vib} at reference temperature (298.15 K) according to the relationship

$$s^{vib} = \int_0^{298.15} \frac{c_p}{T} dT, \tag{9}$$

where c_p is the heat capacity at constant pressure. The excess vibrational entropy $s^{ex,vib}$ of the solid-solution series is obtained from subtracting the vibrational entropy of an ideal solution $s^{vib,id}$ from the measured s^{vib}

$$s^{ex,vib} = s^{vib} - s^{vib,id}, \tag{10}$$

where $s^{vib,id}$ is the weighted average of the end-member vibrational entropies.

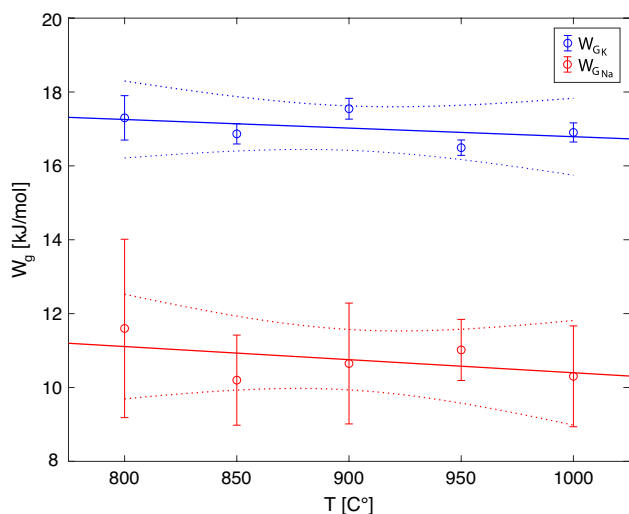


Fig. 1 W_{gK} (blue) and W_{gNa} (red) versus temperature. The vertical bars indicate standard deviations derived as described in the text. The solid lines are the linear least square fits with intercepts W_{hK} , W_{hNa} and slopes W_{sK} and W_{sNa} , respectively. Dashed lines indicate 95% confidence boundaries obtained from the regression model

Results

Mineral chemistry

The major and trace element compositions of the feldspar starting materials are given in Table 1. All four feldspars are K-rich and generally contain very little Ca. Madagascar Orthoclase contains 1.27 wt% Fe_2O_3 , which corresponds to 0.044 a.p.f.u. Fe^{3+} on the T-site (Coombs 1954; Hofmeister and Rossman 1984). V, Z and Zg contain Ba (M: 765 ppm, V: 6559 ppm, Z: 6952 ppm Zg: 4595 ppm) and Sr (M: 49 ppm, V: 1355 ppm, Z: 584 ppm Zg: 901 ppm). M has some Ti (233 ppm), all other element concentrations are $\ll 100$

Table 1 Compositions of the alkali feldspar starting materials in wt% oxide for Na_2O , K_2O , Al_2O_3 , SiO_2 , CaO and Fe_2O_3 as obtained from EPMA and in ppm for Ba, Rb and Sr, which were measured with ICP-MS

wt% ox	M	V	Z	Zg	apfu	M	V	Z	Zg
Na_2O	0.578	1.737	1.633	1.198	Na	0.052	0.156	0.146	0.107
K_2O	15.802	14.052	14.123	14.705	K	0.936	0.828	0.833	0.868
Al_2O_3	17.242	18.960	18.788	18.791	Al	0.944	1.033	1.024	1.024
SiO_2	65.028	64.002	64.346	64.278	Si	3.020	2.957	2.975	2.973
CaO	0.000	0.000	0.011	0.000	Ca	0.000	0.000	0.001	0.000
Fe_2O_3	1.271	0.213	0.028	0.037	Fe	0.044	0.007	0.001	0.001
Ba [ppm]	765	6559	6952	4595	Ba	0.002	0.013	0.014	0.009
Rb [ppm]	162	172	194	473	Rb	0.001	0.001	0.001	0.002
Sr [ppm]	49	1355	584	901	Sr	0.000	0.004	0.002	0.003
Total	100.019	99.773	99.702	99.607	Total	4.999	4.999	4.996	4.987

The sum formulae were calculated based on 5 cations. Charge balance and spectroscopic analysis (Coombs 1954; Hofmeister and Rossman 1984) show that Fe is present as Fe^{3+} in M

ppm. Full mineral chemical analyses are available in the Supplementary Information (Table S2).

Al–Si ordering state

The lattice parameters obtained from pXRD are shown in Table S1. All feldspars are monoclinic with space group $C2/m$, except for samples that were shifted to $X_K < 0.3$ or to $X_K < 0.4$ for Zg adularia, which are metrically triclinic with space group $C\bar{1}$. The state of Al–Si ordering was determined from the ratio b/c^* using the equations for $2t_1$ from Kroll and Ribbe (1987) for monoclinic or triclinic feldspars, respectively. The value t_1 indicates the proportion of the Al-ions on each of the T1 sites where $t_1=0.25$ represents fully disordered and $t_1=0.5$ fully ordered Al–Si. The respective values for $2t_1$ are given in Table S1 and are shown in Fig. S3 in the Supplementary Information. The terms high sanidine (HS), low sanidine (LS), and orthoclase (OR) are used in the following as defined by Ribbe (1983) with HS: $0, 5 < 2t_1 < 0, 666$; LS: $0, 666 < 2t_1 < 0, 74$; OR: $0, 74 < 2t_1 < 1$. Out of the four starting materials, Volkesfeld Sanidine is the most disordered (high sanidine) followed by Madagascar Orthoclase (low sanidine), Zinggenstock and finally Zillertal Adularia (both orthoclase).

Comparison between the starting material and material annealed at 900 °C and at 1000 °C for 35 days reveals a systematic increase of Al–Si-disorder during heat treatment (see Table S1 and Fig. S3). Annealing at 900 °C produced limited disordering with changes of $2t_1$ from 0.689 to 0.673 for M, from 0.611 to 0.603 for V, from 0.874 to 0.842 for Z, and from 0.838 to 0.800 for Zg (see Table S1). The changes in Al–Si ordering state are independent of whether annealing occurred isochemically or was accompanied by cation exchange, and the cation exchange series plot along lines of constant $2t_1$ in Fig. S3. Annealing at 1000 °C produced substantial disordering so that all feldspars changed to high sanidine with $2t_1$ of 0.579 for Z, 0.646 for Zg, 0.524 for M,

and 0.556 for V. Although the feldspars become metrically triclinic when shifted towards Na-rich compositions (see Tab. S1), they remain topochemically monoclinic irrespective of the annealing temperature.

Thermodynamic mixing properties

Excess Gibbs energy of mixing from Na–K partitioning

The compositions of melt, X_{KCl} , feldspar, X_{K} , pairs after cation exchange are plotted in Fig. 2. Despite the 40:1 molar ratio for alkali cations contained in melt and feldspar, the melt undergoes a slight change in its composition during the experiments due to the requirement of mass balance in a closed system. For determining the partitioning of Na–K between melt and feldspar the melt compositions were corrected accordingly (see Fig. S4 in the SI). For each feldspar–melt pair the 1σ standard deviation of the feldspar composition obtained from 5–10 EPMA measurements performed on each sample is indicated. For experiments at 800 °C, the 1σ bars for feldspar compositions are significantly larger than for the experiments performed at 850 °C, 900 °C, 950 °C and 1000 °C indicating incomplete equilibration at 800 °C. Shifting K-rich feldspars to Na-rich composition is accompanied by a strongly anisotropic contraction of the crystal structure. Typically, this leads to fracturing, when the compositional shift exceeds about 15 mole% (Neusser et al. 2012; Scheidl et al. 2013; Petrishcheva et al. 2019; Abart et al. 2022). Through this, new surfaces are generated, which enhance melt–feldspar cation exchange. As a result, the Na-rich feldspars are equilibrated relatively well. As all starting materials are relatively K-rich, only small shifts are required to produce the desired compositions on the K-rich side, which are facilitated merely by intracrystalline Na–K interdiffusion. When the starting materials are shifted to intermediate compositions, the compositional shifts may be too small to induce fracturing, and feldspar–melt equilibrium partitioning is the most difficult to attain. Indeed, the largest compositional variations indicating the least extent of equilibration is observed for Z and Zg shifted to intermediate compositions. After cation exchange at 800 °C M and V appear to be well equilibrated with the salt melt, whereas Z and Zg don't. This difference rather has kinetic than thermodynamic reasons and for the 800 °C experiments only the

partitioning curves obtained for M and V were considered in the thermodynamic analysis.

The partitioning curves produced from cation exchange at 800 °C for M and V and at 850 °C, 900 °C, 950 °C and 1000 °C for all four feldspars are indistinguishable (see Fig. 2). In the thermodynamic analysis we therefore did not discriminate between the partitioning curves obtained for the different feldspars. All melt–feldspar pairs obtained for a given temperature were used to extract the corresponding Margules parameters in a single fitting run. Hovis et al. (1991) and Hovis (2017) suggested to restrict the analysis to feldspar compositions to within the range $0.07 < X_{\text{K}} < 0.91$ since uncertainties for near-end-member compositions are high, and including such compositions could potentially distort the results. Nonetheless, in our study the entire compositional range was used for determining the Margules parameters, as restricting the analysis to feldspar compositions of $0.07 < X_{\text{K}} < 0.91$ did not have any effect on the results. The Margules parameters obtained from fitting Eq. (4) to the partitioning data are given in Table 2, and the corresponding partitioning curves are shown as solid lines in Fig. 2.

The uncertainties given for W_{gK} and W_{gNa} in Table 2 and illustrated in Fig. 1 are standard deviations obtained from selecting feldspar compositions randomised according to mean and standard deviation as determined from EPMA analysis and calculating Margules parameters for each choice of compositions. For details refer to the Supplementary Information.

Even if the W_{gK} and W_{gNa} parameters have considerable associated uncertainties, the mean values indicate a decreasing trend with increasing temperature for both the W_{gK} and W_{gNa} parameters (Fig. 1). The solid lines represent the linear least square fits with slopes W_{sK} , W_{sNa} , and intercepts W_{hK} and W_{hNa} (Eq. (6)), respectively. The W_{h} and W_{s} parameters were used to calculate h^{ex} , s^{ex} and g^{ex} , which are shown in Fig. 3 together with literature data (see figure caption for details).

Low-temperature heat capacity measurements

The excess vibrational entropy obtained from heat capacity measurements by low-temperature calorimetry of 14 samples with different X_{K} of the solid-solution prepared from V is shown in Fig. 4. The excess vibrational entropy is positive

Table 2 Overview of experiments and of the Margules parameters $\pm 1\sigma$ obtained for the different temperatures as described in the text

Temperature	800 °C	850 °C	900 °C	950 °C	1000 °C
Duration [h]	840	840	840	840	672
$\Delta_r g^0$ [J/mol]	10,092 \pm 261	9191 \pm 186	9324 \pm 268	8844 \pm 115	8325 \pm 255
W_{gK} [J/mol]	17,300 \pm 613	16,867 \pm 301	17,547 \pm 270	16,493 \pm 206	16,905 \pm 282
W_{gNa} [J/mol]	11,599 \pm 2434	10,199 \pm 1197	10,649 \pm 1607	11,017 \pm 751	10,303 \pm 1426

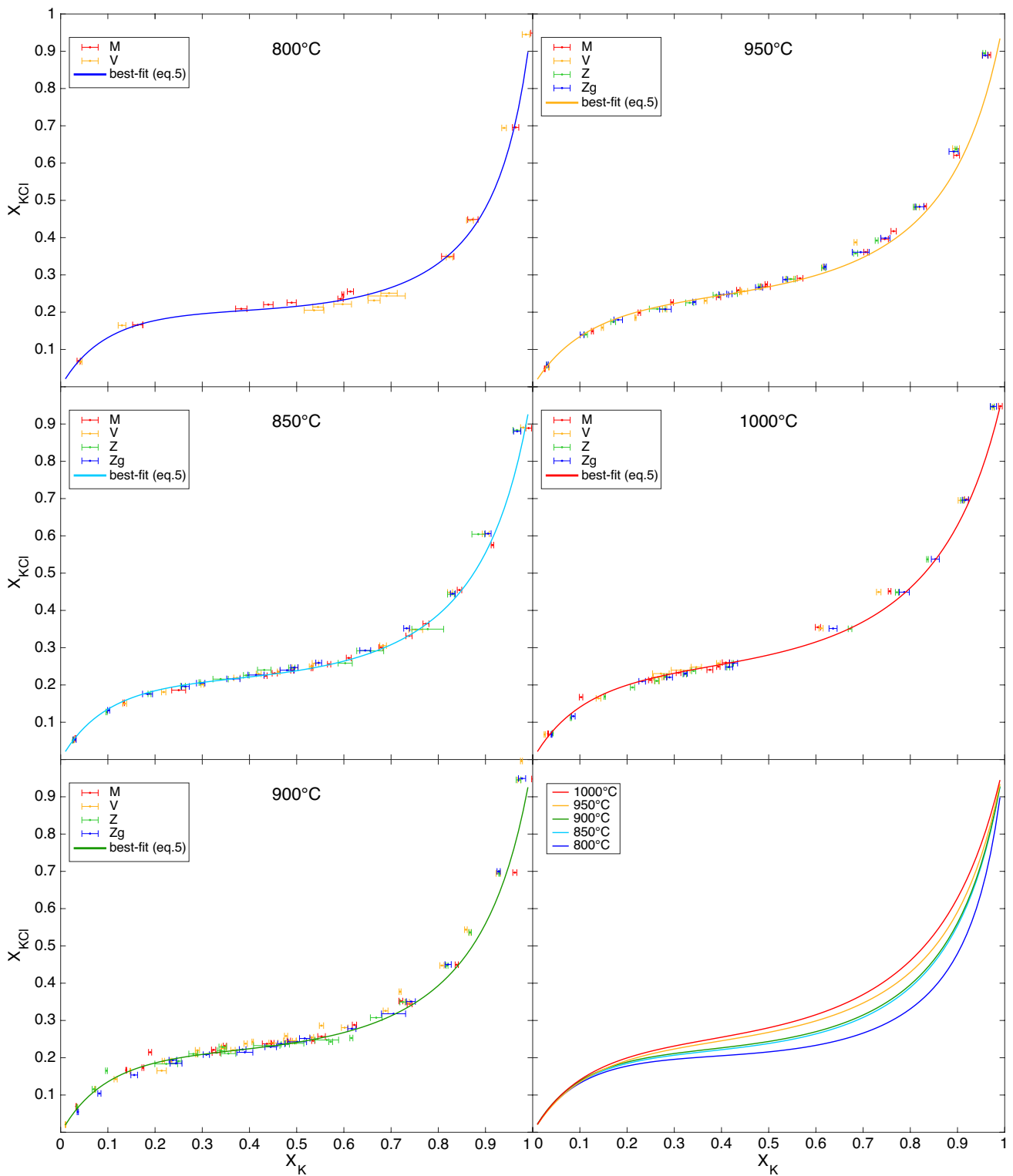


Fig. 2 Melt composition (X_{KCl}) versus feldspar compositions (X_K) for all experiments. Feldspar compositions were measured by EPMA, melt compositions were obtained from the weighted salt mixture and corrected for compositional shift during Na–K exchange with the feldspar in a closed system (see text). The horizontal error bars give

1σ values obtained from replicate EPMA measurements ($5 \leq n \leq 10$) of feldspar in each run product. The solid lines represent the partitioning curves corresponding to the best-fit W_{gK} , W_{gNa} and $\Delta_r g^0$ for each temperature. The partitioning curves obtained for the different temperatures are compared in the bottom right panel

Fig. 3 Comparison of excess enthalpy, h^{ex} , entropy, s^{ex} and Gibbs energy, g^{ex} , from this study with literature data: feldspars with Al–Si highly ordered, intermediate ordering and highly disordered feldspars are shown with dotted, dashed and solid lines, respectively. **a** h^{ex} from this study (magenta) compared with results from [1] Hovis (1988), [2] Delbove (1975), [3] Waldbaum and Robie (1971), [4] Hovis et al. (1991), [5] Hovis (2017), [6] Delbove (1975). **b** Curves for s^{ex} (green), $s^{ex,vib}$ (grey) and $s^{ex,con}$ (magenta), results for this study were obtained as described in the text. Literature data is as follows: $s^{ex,vib}$ was taken from Haselton et al. (1983); Benisek et al. (2014), s^{ex} from Hovis et al. (1991); Hovis (2017). **c** Curves for g^{ex} at 800 °C from this study (magenta) and literature as described in the legend

over the entire compositional range with a maximum of about $2 \text{ J} \cdot \text{mol}^{-1} \cdot \text{K}^{-1}$. The same two parameter sub-regular mixing model as used for fitting g^{ex} was used for obtaining the W_s^{vib} parameters from the $s^{ex,vib}$ data by least square fitting, the best-fit W_s^{vib} parameters are given in Table 3. The $s^{ex,vib}$ curve is nearly symmetrical with respect to composition with the maximum at $X_K = 0.4$. Based on the notion that excess entropy is the sum of the vibrational and the configurational contribution, $s^{ex} = s^{ex,vib} + s^{ex,con}$, the configurational contribution, $s^{ex,con}$, to the excess entropy can be obtained by subtracting $s^{ex,vib}$ from s^{ex} . The W_{sK}^{con} and W_{sNa}^{con} parameters obtained this way are given in Table 2, and the $s^{ex,con}$ curve is shown in Fig. 3.

Discussion

The partitioning data depicted in Fig. 2 are reproduced very well by the calculated partitioning curves indicating that the chosen two parameter Margules model is well suited for describing the thermodynamic non-ideality of the alkali feldspar solid-solution. Qualitatively, non-ideality of the alkali feldspar solid-solution can be inferred from the fact that the partitioning curves show an inflection point. Given that the salt-melt has practically ideal thermodynamic mixing properties at the temperatures of the cation exchange experiments (Hersh and Kleppa 1965; Yin et al. 2020), an inflection point in the partitioning curves is an unambiguous indication for non-ideality of the alkali feldspar solid-solution. With increasing temperature, the slope of the partitioning curve at the inflection point increases indicating decreasing non-ideality of the feldspar solid-solution with increasing temperature.

The fact that partitioning at a given temperature is similar for all four feldspars indicates that equilibrium element partitioning between alkali feldspar and NaCl–KCl salt melt is independent of the Al–Si ordering state and of the minor and trace element compositions over the ranges covered by the four feldspar starting materials and the corresponding run products. Through the large number of partitioning data considered for extraction of the Margules parameters at each temperature the W_{gNa} and W_{gK} parameters are well

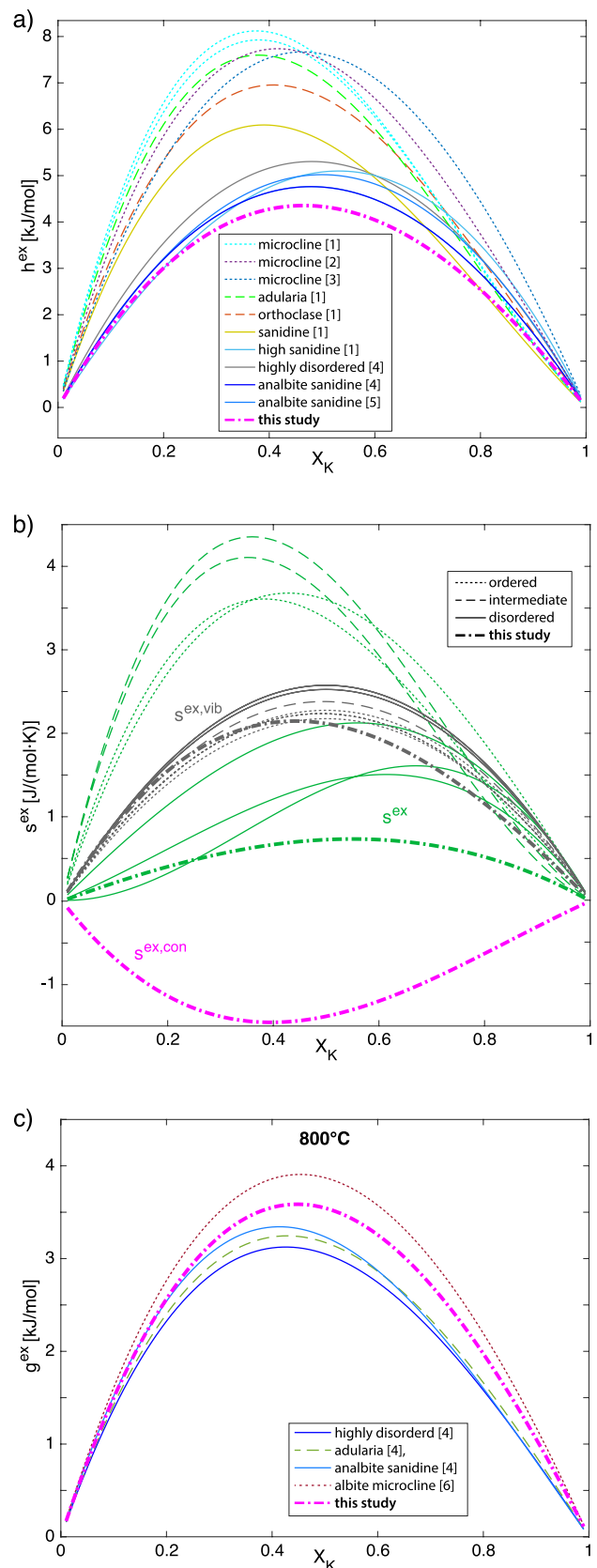


Table 3 Excess enthalpy h^{ex} and entropy s^{ex} as obtained from the partitioning experiments and $s^{ex,vib}$ from low-temperature calorimetric heat capacity measurements and excess configurational entropy $s^{ex,con}$ as obtained from the difference between $s^{ex,vib}$ and s^{ex}

Quantity	W_K	W_{Na}
h^{ex} [J/mol]	$19,754 \pm 3140$	$14,916 \pm 4272$
s^{ex} [J/(mol·K)]	2.33 ± 2.67	3.55 ± 3.64
$s^{ex,vib}$ [J/(mol·K)]	10.51	6.43
$s^{ex,con}$ [J/(mol·K)]	-8.18	-2.88

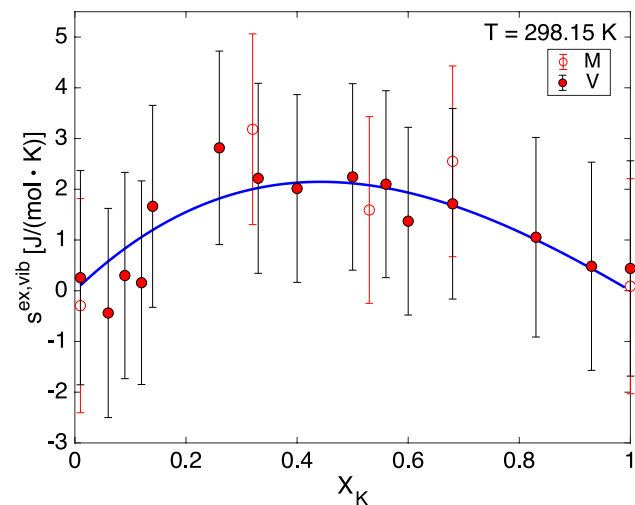


Fig. 4 Excess vibrational entropy; filled red circles are $s^{ex,vib}$ obtained from low-temperature c_p data of samples prepared from V, empty red circles indicate data of samples prepared from M with respective 1σ standard deviation. The solid line is the best-fit using Eq. (7) based on the V data

constrained. The 1σ standard deviations indicated in Fig. 1 were obtained from multiple fitting runs, where for successive fitting runs each feldspar composition was calculated from Monte Carlo experiments based on the mean value and standard deviation obtained from replicate EPMA measurements of the respective feldspar. Comparison with literature data as shown in Fig. 3a reveals good agreement between h^{ex} derived from our partitioning experiments and the results from solution calorimetry. The latter show increasing h^{ex} and increasing asymmetry of the h^{ex} curve with increasing Al–Si ordering state. The h^{ex} derived from our study is close to h^{ex} of disordered feldspars as given by Hovis (1988); Hovis et al. (1991) and Hovis (2017).

Previous studies that covered a broad range of Si–Al ordering states ranging from the fully ordered low-albite microcline series to the fully disordered monalbite - sanidine series, found that the alkali feldspar solid-solution becomes increasingly more non-ideal with increasing state of Si–Al ordering (see Fig. 3). This is in line with experimentally determined two-feldspar equilibrium phase relations, which

reveal immiscibility up to 900 °C (Bachinski and Müller 1971) for ordered feldspars, and up to about 600 °C for disordered feldspars (Smith and Parsons 1974; Sipling and Yund 1976; Parsons 1978). This has been ascribed to the fact, that Al–Si disordering increases the unit cell volume and facilitates mixing of the differently sized Na^+ and K^+ cations on the alkali cation site (Benisek et al. 2014; Hovis 2017), an effect that is qualitatively similar to the influence of increasing temperature. Based on solution calorimetry Hovis (2017) found a correlation between the maximum h^{ex} and the state of Al–Si ordering expressed as Z , with $Z = X_{Al}^{T1o+T1m} - X_{Al}^{T2o+T2m}$ (Thompson 1969).

Such a correlation is missing in the feldspars investigated in our study. Interestingly, the W_{gK} , W_{gNa} parameters calculated from the data of Hovis (2017) for the Al–Si ordering states of our feldspars are almost identical to those obtained from our partitioning experiments. According to literature data, the excess entropy s^{ex} of alkali feldspar solid-solution is independent of the Al–Si ordering state. Positive $s^{ex,vib}$ has been reported for both ordered (Benisek et al. 2014) and disordered (Haselton et al. 1983) alkali feldspar solid-solutions (see Fig. 3b). In both studies, $s^{ex,vib}$ was obtained from positive excess heat capacities measured by low-temperature calorimetry and additionally by differential scanning calorimetry (DSC) between 273 K and 773 K by Benisek et al. (2014). For pure end-members, heat capacities were determined with DSC between 350 K and 1000 K by Hemingway et al. (1981). In alkali feldspars, only Na- and K- vibrations, which are stimulated at low temperatures, contribute to $s^{ex,vib}$. Therefore, $s^{ex,vib}$ remains constant above about 200 K (Benisek et al. 2015). Also in plagioclase feldspars, $s^{ex,vib}$ is more or less independent of T above 298 K, where, in contrast to alkali feldspars, high-frequency vibrations of tetrahedrons can play a role (Benisek et al. 2009). However, $s^{ex,vib}$ obtained from low temperature calorimetry is applicable to the temperatures at which the experiments were performed (Benisek et al. 2015). The positive excess heat capacity and inferred excess vibrational entropy was ascribed to the increase of Na–O bond lengths and associated weakening of the bond with increasing X_K , where the maximum effect is expected at intermediate compositions (Benisek et al. 2014, 2015). We determine positive $s^{ex,vib}$ for V with maximum values of $s^{ex,vib}$ of about $2 \text{ J} \cdot \text{mol}^{-1} \cdot \text{K}^{-1}$ for intermediate compositions and with a similar, though less well constrained trend for M. For our data, comparison between s^{ex} and $s^{ex,vib}$ yields negative $s^{ex,con}$ at every composition (Fig. 3b) with a minimum at $X_K=0.4$. Negative excess entropy may be due to K–Na short range ordering, an inference that is corroborated by independent evidence for clustering of alkali cations in alkali feldspar (Phillips et al. 1988; Angel et al. 2013; Sanchez-Munoz et al. 2013).

All investigated feldspars slightly differ from pure binary solid-solutions due to incorporation of minor and trace

elements (see Tables 1 and S2). For example, V, Z, and Zg have considerable celsian component with Ba present at concentrations of 0.013–0.016 a.p.f.u., and M has 0.044 a.p.f.u. Fe^{3+} on the tetrahedral site. None of these impurities seems to have a measurable effect on the Na–K partitioning between salt-melt and alkali feldspar, though. The fact that V and Zg, which have similar minor element composition but different Al–Si-ordering state, show similar Na–K partitioning renders it unlikely that the effects of minor elements and Al–Si ordering state cancel each other out. This is why we infer that neither variations of the Al–Si ordering state nor the variations in minor and trace element contents exhibited by the four feldspars used in our study and by the corresponding run products have a measurable influence on the Na–K partitioning between alkali feldspar and NaCl–KCl salt melt at temperatures between 800 °C to 1000 °C and at close to ambient pressure.

The solvus curves calculated for 1bar and for 1kbar based on our calibration of the Margules parameters and with the pressure effect for the 100 MPa solvus considered using the W_V parameters of Hovis et al. (1991) are shown in Fig. 5.

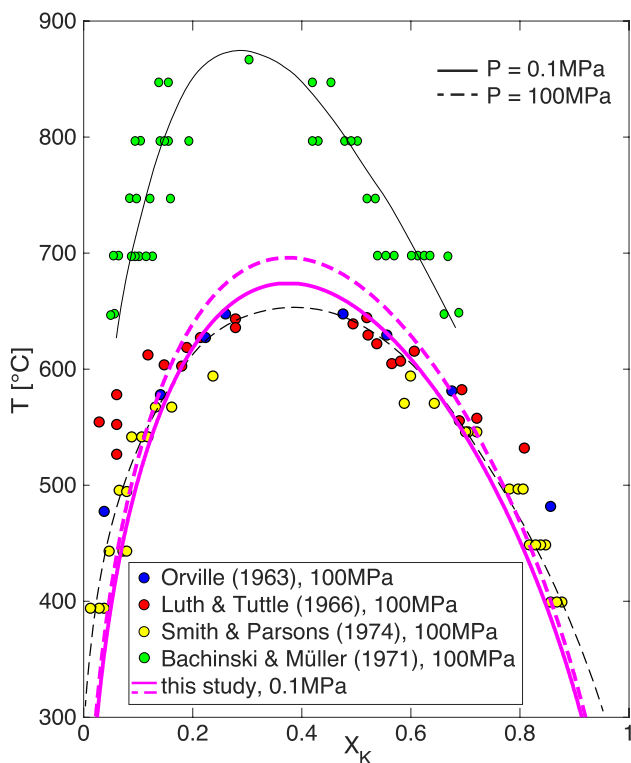


Fig. 5 Solvi at 0.1 MPa (solid lines) and at 100 MPa (dashed lines). Magenta lines are the solvi obtained from the thermodynamic data of this work, black lines are taken from Bachinski and Müller (1971) (ordered Al–Si) and Smith and Parsons (1974) (disordered Al–Si) with the respective experimental data as described in the legend. The experimental data of Orville (1963) and Luth and Tuttle (1966) was performed at 200 MPa but is shown as adjusted to 100 MPa by Smith and Parsons (1974)

Our solvus curves are compared with 100 MPa phase equilibrium data for disordered feldspars from Orville (1963); Luth and Tuttle (1966); Smith and Parsons (1974) and with 0.1 MPa phase equilibrium data for ordered feldspar from Bachinski and Müller (1971). The solvus curve obtained from our calibration is very similar to the ones given for disordered feldspars by Orville (1963); Luth and Tuttle (1966); Smith and Parsons (1974). The experimental data from Orville (1963); Smith and Parsons (1974) are very well reproduced by these solvus curves. Only the experimental data of Luth and Tuttle (1966) indicate a somewhat more asymmetric solvus with a steeper limb on the Na-rich side than the calculated solvus curves. There does not seem to be any systematic variation in the experimental data of Orville (1963); Luth and Tuttle (1966); Smith and Parsons (1974) that would allow to discern an effect of the Al–Si ordering state on the solvus, which is in line with our findings. Only the solvus curve given for ordered alkali feldspar of the low-albite - microcline series by Bachinski and Müller (1971) exhibits a substantially larger miscibility gap indicating the effect of highly ordered Al–Si. In contrast to the previous studies, which are based on phase equilibria at temperatures below the critical temperature of the solvus for disordered alkali-feldspar, our analysis is based exclusively on phase equilibria observed at temperatures above the critical temperature of the solvus for disordered alkali feldspar. The fact that extrapolation of g^{ex} and its temperature dependence obtained from Na–K partitioning at temperatures between 800 °C and 1000 °C reproduces phase equilibria that were experimentally determined at substantially lower temperatures suggests that the high-temperature partitioning experiments provide independent constraints on equilibrium phase relations in the alkali feldspar system even at lower temperatures, where attainment of equilibrium may be difficult in experiment.

Conclusions

The equilibrium partitioning of Na and K between alkali feldspar and NaCl–KCl salt melt was investigated experimentally at temperatures between 800 °C and 1000 °C and at a pressure of close to 0.1 MPa. Four different starting materials with Al–Si ordering states characterised by $0.6 \leq 2t_1 \leq 0.9$, where $2t_1$ is the T_1 site fraction of Al^{3+} , and slightly different minor and trace element compositions all yield similar partitioning curves indicating that neither the state of Al–Si ordering nor the minor and trace element concentrations have a measurable influence on Na–K partitioning over the range of Al–Si ordering states and minor element contents covered by the starting materials and the respective run products. From the thermodynamic analysis of the partitioning data the excess Gibbs energy accounting

for the non-ideality of the alkali feldspar solid-solution including its temperature dependence were obtained. The corresponding solvus curve is slightly skewed to the Na rich side with a critical temperature of somewhat above 650 °C at $X_K = 0.39$, which is well comparable with literature data for low sanidine solvus. Comparison of excess vibrational entropy derived from heat capacity measurements by low-temperature calorimetry with the excess entropy obtained from the temperature dependence of the excess Gibbs energy yields negative configurational contributions to the excess entropy indicating clustering of Na and K on the alkali site. From the good agreement between the solvus curve obtained from Na–K partitioning experiments performed at temperatures well above the critical temperature of the solvus with two-feldspar phase equilibria determined by experiments performed at temperatures below the critical temperature of the solvus it is concluded that the high-temperature partitioning experiments provide valid and independent constraints on two feldspar equilibria.

Supplementary Information The online version contains supplementary material available at <https://doi.org/10.1007/s00269-024-01270-z>.

Acknowledgements This study was funded by the Austrian Science foundation, FWF Grant No. I 4404 to R. Abart and by FWF grant P33904 to E. Dachs. We gratefully acknowledge the thorough reviews by Guy Hovis and an anonymous reviewer, and we thank Jamie Connolly for fruitful discussions.

Author contributions R.A. did the conceptualization of the project, D.H. carried out the experiments, E.P. contributed to the calculations, F.I. and E.D. performed the calorimetric measurements, C.L. did the pXRD analyses, C.H. did the ICP-MS analyses.

Funding Open access funding provided by University of Vienna. This study was funded by the Austrian Science foundation, FWF Grant No. I 4404 and by FWF grant P33904 to E. Dachs.

Availability of data and materials All relevant data is given in the supplementary information.

Declarations

Conflict of interest The authors declare no competing interests.

Open Access This article is licensed under a Creative Commons Attribution 4.0 International License, which permits use, sharing, adaptation, distribution and reproduction in any medium or format, as long as you give appropriate credit to the original author(s) and the source, provide a link to the Creative Commons licence, and indicate if changes were made. The images or other third party material in this article are included in the article's Creative Commons licence, unless indicated otherwise in a credit line to the material. If material is not included in the article's Creative Commons licence and your intended use is not permitted by statutory regulation or exceeds the permitted use, you will need to obtain permission directly from the copyright holder. To view a copy of this licence, visit <http://creativecommons.org/licenses/by/4.0/>.

References

- Abart R, Petrishcheva E, Habler G, Sutter C, Fischer FD, Predan J, Kegl M, Rammerstorfer FG (2022) Evolution of chemically induced cracks in alkali feldspar: thermodynamic analysis. *Phys Chem Miner* 49(5):14–14
- Angel RJ, Ross NL, Zhao J, Sochalski-Kolbus L, Krueger H, Schmidt BC (2013) Structural controls on the anisotropy of tetrahedral frameworks: the example of monoclinic feldspars. *Eur J Mineral (Stuttgart)* 25(4):597–614
- Bachinski SW, Müller G (1971) Experimental determinations of the microcline–low albite solvus. *J Petrol* 12(2):329–356
- Benisek A, Dachs E, Kroll H (2009) Excess heat capacity and entropy of mixing in high structural state plagioclase. *Am Mineral* 94(8–9):1153–1161
- Benisek A, Dachs E, Kroll H (2014) Thermochemistry of the alkali feldspars: calorimetric study of the entropy relations in the low albite–low microcline series. *Am Mineral* 99(1):76–83
- Benisek A, Dachs E, Grodzicki M (2015) First-principles investigation of the lattice vibrations in the alkali feldspar solid solution. *Phys Chem Miner* 42(3):243–249
- Connolly J (2005) Computation of phase equilibria by linear programming: a tool for geodynamic modeling and its application to subduction zone decarbonation. *Earth Planet Sci Lett* 236(1–2):524–541
- Coombs DS (1954) Ferriferous orthoclase from Madagascar. *Mineral Mag* 30(226):409–427
- Dachs E, Bertoldi C (2005) Precision and accuracy of the heat-pulse calorimetric technique: low temperature heat capacities of milligram-sized synthetic mineral samples. *Eur J Mineral (Stuttgart)* 17(2):251–259
- Delbove F (1975) Excess Gibbs energy of microcline - low albite alkali feldspars at 800 °c and 1 bar, based on fused alkali bromide ion exchange experiments. *Am Mineral* 60(11–1):972–984
- Goldsmith JR, Newton RC (1974) An experimental determination of the alkali feldspar solvus. In: MacKenzie WS, Zussman J (eds) *The feldspars*. Manchester University Press Manchester, pp 337–359
- Haselton HT, Hovis GL, Hemingway BS, Robie RA (1983) Calorimetric investigation of the excess entropy of mixing in analbite–sanidine solid solutions: lack of evidence for na, k short-range order and implications for two-feldspar thermometry. *Am Mineral* 68(3–4):398–413
- Hemingway BS, Krupka KM, Robie RA (1981) Heat capacities of the alkali feldspars between 350 and 1000 k from differential scanning calorimetry, the thermodynamic functions of the alkali feldspars from 298.15 to 1400 k, and the reaction quartz + jadeite = analbite. *Am Mineral* 66(11–12):1202–1215
- Hersh LS, Kleppa O (1965) Enthalpies of mixing in some binary liquid halide mixtures. *J Chem Phys* 42(4):1309–1322
- Hofmeister AM, Rossman GR (1984) Determination of fe³⁺ and fe²⁺ concentrations in feldspar by optical absorption and epr spectroscopy. *Phys Chem Miner* 11(5):213–224
- Holland TJB, Powell R (1998) An internally consistent thermodynamic data set for phases of petrological interest: an internally consistent thermodynamic data set. *J Metamorph Geol* 16(3):309–343
- Holland TJB, Powell R (2011) An improved and extended internally consistent thermodynamic dataset for phases of petrological interest, involving a new equation of state for solids. *J Metamorph Geol* 29(3):333–383
- Hovis GL (1988) Enthalpies and volumes related to K–Na mixing and Al–Si order/disorder in alkali feldspars. *J Petrol* 29(4):731–763

- Hovis GL (2017) A refined view of the thermodynamic mixing quantities for alkali feldspars and the quandary of excess configurational entropy. *Am J Sci* 317(5):597–640
- Hovis GL, Delbove F, Roll Bose M (1991) Gibbs energies and entropies of K–Na mixing for alkali feldspars from phase equilibrium data: implications for feldspar solvi and short-range order. *Am Mineral* 76(5–6):913–927
- Kroll H (1971) Determination of Al, Si distribution in alkali feldspars from X-ray powder data. *Neues Jb Miner Monat*, pp 91–94
- Kroll H, Ribbe PH (1987) Determining (Al, Si) distribution and strain in alkali feldspars using lattice parameters and diffraction-peak positions; a review. *Am Mineral* 72(5–6):491–506
- Kroll H, Schmiemann I, Cölln G (1986) Feldspar solid solutions. *Am Mineral* 71:1–16
- Lagache M, Weisbrod A (1977) The system: two alkali feldspars–KCl–NaCl–H₂O at moderate to high temperatures and low pressures. *Contrib Mineral Petrol* 62(1):77–101
- Luth W, Tuttle O (1966) Alkali feldspar solvus in the system Na₂O–K₂O–Al₂O₃–SiO₂–H₂O. *Am Mineral* 51(9–10):1359
- Margules M (1895) Über die Zusammensetzung der gesättigten Dämpfe von Mischungen. *Sitzungsberatungen Akad Wiss Wien Math-Nat Klasse* 104:1243–1278
- Neusser G, Abart R, Fischer F, Harlov D, Norberg N (2012) Experimental Na/K exchange between alkali feldspar and an NaCl–KCl salt melt: chemically induced fracturing and element partitioning. *Contrib Mineral Petrol* 164:341–58
- Orville PM (1963) Alkali ion exchange between vapor and feldspar phases. *Am J Sci* 261(3):201–237
- Orville PM (1967) Unit-cell parameters of the microcline-low albite and the sanidine-high albite solid solution series. *Am Mineral* 52(1–2):55–86
- Parsons I (1978) Alkali-feldspars: which solvus? *Phys Chem Miner* 2(3):199–213
- Petrishcheva E, Rieder M, Predan J, Fischer FD, Giester G, Abart R (2019) Diffusion-controlled crack propagation in alkali feldspar. *Phys Chem Miner* 46(1):15–26
- Phillips BL, Kirkpatrick R, Hovis GL (1988) Al, Si, and Na mas NMR study of an Al, Si ordered alkali feldspar solid solution series. *Phys Chem Miner* 16(3):262–275
- Redlich O, Kister AT (1948) Algebraic representation of thermodynamic properties and the classification of solutions. *Ind Eng Chem* 40(2):345–348
- Ribbe PH (1983) Chemistry, structure and nomenclature of feldspars. In: Ribbe PH (ed) *Feldspar mineralogy*. Reviews in mineralogy. Mineralogical Society of America, Chantilly, Virginia, pp 1–19
- Sanchez-Munoz L, Sanz J, Sobrados I, Gan Z (2013) Medium-range order in disordered k-feldspars by multinuclear NMR. *Am Mineral* 98(11–12):2115–2131
- Scheidl KS, Schäffer AK, Petrishcheva E, Habler G, Fischer FD, Schreuer J, Abart R (2013) Chemically induced fracturing in alkali feldspar. *Phys Chem Miner* 41:1–6
- Sipling PJ, Yund RA (1976) Experimental determination of the coherent solvus for sanidine-high albite. *Am Mineral* 61:897–906
- Smith P, Parsons I (1974) The alkali-feldspar solvus at 1 kilobar water-vapour pressure. *Mineral Mag* 39(307):747–767
- Thompson JB (1967) Thermodynamic properties of simple solutions. *Researches in geochemistry*. Wiley, New York, pp 340–361
- Thompson JB (1969) Chemical reactions in crystals. *Am Mineral* 54:341–375
- Thompson JB, Waldbaum DR (1968) Mixing properties of sanidine crystalline solutions: I. calculations based on ion-exchange data. *Am Mineral* 53(11–1):1965
- Waldbaum DR, Robie RA (1971) Calorimetric investigation of Na–K mixing and polymorphism in the alkali feldspars. *Z Krist-Cryst Mater* 134(1–6):381–420
- Waldbaum DR, Thompson JB (1968) Mixing properties of sanidine crystalline solutions: [part] 2, calculations based on volume data. *Am Mineral* 53(11–12):2000–2017
- Yin H, Lin J, Hu B, Liu W, Guo X, Liu Q, Tang Z (2020) Thermodynamic description of the constitutive binaries of the NaCl–KCl–UCl₃–PuCl₃ system. *Calphad* 70:101783

Publisher's Note Springer Nature remains neutral with regard to jurisdictional claims in published maps and institutional affiliations.